Insight of holey-graphene in the enhancing of electrocatalytic activity as supporting material

To cite this article before publication: Hongjun You *et al* 2018 *Nanotechnology* in press https://doi.org/10.1088/1361-6528/aad7a2

Insight of holey-graphene in the enhancing of electrocatalytic activity as supporting material

Hongjun You,[1,2] Yingying Xuan,[3,4] Yun Zuo,[1] Fei Shen,[3,4] Xiaogang Han,[3,4] and Jixiang Fang[2]

1 School of Science, Xi'an Jiaotong University, Xi'an, Shaanxi 710049, P. R. China

2 Key Laboratory of Physical Electronics and Devices of Ministry of Education, School of Electronic and Information Engineering, Xi'an Jiaotong University, Xi'an, Shaanxi 710049, P. R. China

3 Center of Nanomaterials for Renewable Energy, State Key Lab of Electrical Insulation and Power Equipment, Xi'an Jiaotong University, Xi'an, Shaanxi 710049, P. R. China

4 Key Lab of Smart Grid of Shaanxi Province, Xi'an, Shaanxi 710049, China

E-mail: xiaogang.han@xjtu.edu.cn and jxfang@mail.xjtu.edu.cn

Abstract:

An ideal supporting material improves both activity and durability of noble-metal nanoparticles in electrocatalytic reactions. Graphene possesses a high transport rate of electrons in-plane, a low cost, and stability, but, the restacking of graphene layers trap noble-metal nanoparticles and make them inaccessible to reactants and results in reduced catalytic activity. Here, holey-graphene as the supporting materials for Pt nanoparticle catalysts is deeply investigated in the electrocatalytic reaction of methanol oxidation (MOR). The holey-graphene can be scalable to synthesize using our simple method described herein. The holes on the holey-graphene layer promote the access of reactants with Pt nanoparticle catalysts compared with carbon black and graphene when used as supporting materials. Density functional theory (DFT) calculations and molecule dynamic (MD) simulation further explain the function of holey-graphene in the promotion of electrocatalytic activity. Holey-graphene may open extraordinary possibilities as a supporting material for electrocatalysts.

Keywords: Holey graphene, Electrocatalyst, Methanol oxidation reaction, Electrocatalyst support, Platinum nanocrystals

1. Introduction

Nanosized noble metal particles are the most commonly used catalysts in electrochemical reactions for energy transformation.[1-5] For example, the anode and cathode reactions in polymer electrolyte membrane fuel cells (PEMFCs) are catalysed by Pt or Pd noble metals. The reactions such as the methanol oxidation reaction (MOR), ethanol oxidation reaction, formic acid oxidation reaction, oxygen reduction reaction (ORR), and so on, are greatly promoted by these catalysts.[6-14] To prevent the significant loss of noble metal catalysts in electrochemical surface area (ECSA) due to the aggregation and Ostwald ripening during the reactions, the NPs are usually separated and supported on supporting materials such as carbon materials. As supporting materials some properties are required such as the high electrical conductivity, the appropriate pore structure, the high specific surface area, the excellent crystallinity, and the stable surface properties in aqueous solution system.[15] The long-term performance and durability of the carbon supported catalysts are usually affected by carbon corrosion. The sites that anchor noble metal NPs will decrease induced by carbon corrosion. Thus, the detachment and aggregation of noble metal NPs will happen and lead to structural collapse of the electrode in an extreme case.[16] To achieve the reliability of PEMFC in widespread use, the development of high activity electrocatalysts dispersed on inexpensive supports with high electric conductivity and corrosion-resistance is necessary.

High conductivity carbon blacks (CBs) such as Ketjen Black, Vulcan XC-72R, Black Pearl 2000, Shawinigan, and Denka Black possess turbostratic structures with high surface areas and are widely used as supports for electrocatalyst metal NPs due to their low cost and easy availability.[17] The organo-sulfur groups and micropores on CBs will result in poor utilization and aggregation of metal NPs. The degradation of the catalyst also can be induced by the thermochemical instability

of CBs in the actual catalytic conditions in fuel cells.[18,19] These drawbacks to carbon black will limit the performance the electrocatalysts.[20]

Over the last decade or so, plenty of nanomaterials other than CBs have been developed as support materials for noble metal catalysts, including carbon based support nanomaterials and non-carbonaceous support nanomaterials.[17] Carbon based support nanomaterials such as the carbon nanotubes (CNTs), the mesoporous carbon, the graphene and the carbon nanofibers (CNFs), possess properties like the good stability, the high specific surface area, and the high electrical conductivity.[21-24] Among them, graphene possesses a high in-plane electron transport rat and low cost compared with CNTs, thus, it has attracted more research interest as catalyst support.[16,25-29]Various noble-metal nanocatalysts, such as Pt-on-Pd nanodendrites,[30] PtPd@Pt NPs,[31] PtPd concave nanocubes,[32] PtPd dendritic NPs,[33] star-shaped Pd@Pt NPs,[34] and PtPd nanowires[35] have been investigated by using the graphene as supports. Paul Alivisatos and coworkers have reported that the layers of graphene will attach each other and will prevent or limit molecular and ion diffusion between layers of graphene.[36] Similar results have been reported in porous carbon supporting materials. The noble-metal catalyst NPs would be trapped deeply in recesses or micropores and made inaccessible to reactants, result in the decrease of catalytic activities.[17]

Due to the huge specific surface area and high conductivitythe two dimensional (2D) nanomateirals have attracted great interest in many research fields.[37-39] The restacking problem of graphene has been encountered by researchers in Li ion storage, ultracapacitors, and electrochemical catalysis. To overcome graphene restacking, graphene foam,[40] graphene frameworks,[41] sponge-like graphene,[42] and holey graphene[43-45] have been developed as electrode materials or supporting materials for metal nanocatalysts. However, as supports, the restacking effect of graphene on the

electrocatalytic properties of noble metal NPs has not been deeply investigated. In our previous work, a simple method has been developed for the scalable holey graphene synthesis and obtained high performance in ultracapacitors.[46] In this paper, we study the restacking problem of graphene and the holey graphene as a new kind of supporting material in overcoming the restacking problem in electrocatalytic systems. The methanol oxidation reaction (MOR) canalized by Pt NPs catalyst was selected as a model reaction system to investigate the properties of graphene and holey graphene as supporting materials. The unique nanostructure of holey graphene as supports for Pt NP enabled higher catalytic activity than the graphene and carbon black and indicates that holey graphene can overcome the restacking problem and improve the catalytic properties of noble metal NPs.

2. Methods section

2.1 Synthesis of holey graphene

The synthesis of holey grapheme is similar with our previous report.[46] In a typical reaction, 200 mg starting graphene (Vor-X from Vorbeck Materials; grade, reduced 070; lot, BK-77x) was heated in air using an open-ended tube furnace (Thermolyne 21100) through placed in an alumina crucible. The increase rate of temperature is 10 ℃/min. Then, the tube furnace was held at 430 ℃ isothermally for 3 hours. After the tube furnace was naturally cooled down to room temperature, the holey graphene was obtained.

2.2 Synthesis of Pt NP catalysts

Specifically, 1 ml chloroplatinic acid hexahydrate (H_2PtCl_6 $6H_2O$, purchased from Aldrich) aqueous solution (30 mM) was mixed with 18 ml deionized water (DI water, 18 MU cm, Millipore) in a 50-ml three-neck flask under magnetic stirring (rotation rate of magnetic bar was 700 rpm). Following, 25 mg Poly(N-vinyl-2-pyrrolidone) (PVP-K30, molecular weight 30000-40000) was

added into the solution. After keeping rotation of 5 minutes, 4.5 ml freshly prepared sodium borohydride ($NaBH_4$) aqueous solution (40 mM) was put into the solution. The solution was kept 12 hours under magnetic stirring with the color changing from colourless to black. The Pt NPs was produced in the solution. Following, this mixture solution was used for the preparation of supported Pt NPs catalysts.

The preparation of the supported Pt NPs catalysts is similar with our previous report.[47,48] Firstly, 2.4 mg supporting materials, i.e. carbon black (Vulcan® XC-72), graphene (Vor-X from Vorbeck Materials), and holey-graphene (synthesized in this work), were separately dispersed in 10 ml ethanol solution in three 20 ml scintillation vials, with 30 minutes sonication. Then, 6 ml aqueous solution containing 0.6 mg Pt NPs (measured by the inductively coupled plasma atomic emission spectroscopy (ICP-AES)) was put into the mixture solution for further 10 minutes sonication. Following the solution was kept stirring for 24 hours. Finally, the product was collected using centrifugation (5000 rpm) and washed with ethanol 3 times. Thus the catalysts that Pt NPs loaded on carbon black (Pt/C), graphene (Pt/G), and holey graphene (Pt/HG) were obtained.

2.3 Characterization of structure and morphology

The morphology of the graphene, holey-graphene and their Pt NPs loaded samples was characterized by transmission electron microscopy (TEM) (JEOL JEM-2100) with an accelerating voltage of 200 kV. The Raman spectrum measurements of the graphene and holey-graphene were carried out on a Horiba Yvon LabRam ARAMIS confocal Raman spectrometer with a 633 nm He–Ne laser line (10 mW). The signal collection time was 10 s and 2 times of acquisition with 2 μm laser beam spot size and power of laser beam being adjusted to 0.1mW.

2.4 Measurement of electrocatalytic properties

Using a VersaSTAT 3 electrochemical working station, the electrocatalysis measurement was performed in a three-electrode cell. The samples were loaded on a glassy-carbon rotating disk electrode (GCE, 5 mm in diameter) and used as the working electrode. A 1 cm×1 cm platinum foil and a double junction Ag/AgCl electrode were used as the counter electrode and the reference electrode, respectively. The working electrode was prepared as following procedure. Firstly, the supported Pt NP catalysts (Pt/HG, Pt/G and Pt/C) were dispersed in DI water with 10 min sonication. Following, 15 μl water suspensions was dripped onto the surface of the GCE and dried naturally. After the evaporation of water, a quantity of 10 μl Nafion solution (0.05 wt %, diluted with mixture solution of DI water and isopropanol from 5 wt % Nafion, Ion Power, Inc.) was covered on the surface and dried naturally to attach the catalyst on to the surface of GCE. All of the electrocatalysis measurements were carried out at room temperature (25 ℃). The ECSA were calculated by integrating the charge of hydrogen adsorption from the cyclic voltammetry (CV) curve which was measured in the argon-saturated 0.1 M $HClO_4$ aqueous solution (diluted from the stock $HClO_4$ solution (70.0% to 72.0%, Tianjin Xinyuan Chemical Reagent)). The catalytic property for MOR was measured in an oxygen-free $HClO_4$ (0.1 M) aqueous solution (bubbled 30 mints with nitrogen) containing different concentrations of methanol (HPLC grade, 99.0%; Aladdin Reagent).

2.5 Method of density functional theory (DFT) calculation

Typically, the DFT calculation was carried out using Dmol3 code.[49] Based on the generalized gradient approximation (GGA), the Perdew-Wang exchange-correlation function (PW91) was used to optimize the adsorption structures of molecules or ions on the Pt and graphene surfaces.[50] The symmetry and spin restrictions were not applied in the structure DFT optimization. The multipolar expansion of charge density and Coulomb potential was described by using a double numerical basis

set with polarization p-function, octupole scheme and DFT semicore pseudopots. The criteria for the obtained final structure were set as following: 1) the maximum displacement per atom and the correlated force due to the displacement should be less than 0.005 Å and 0.002 Ha/Å, respectively; 2) the convergence tolerance of self-consistent field energy should be less than 10^{-6} hartree (Ha; 2.72×10^{-5} eV) in the conjugate gradient algorithm.. The adsorption energy (E_a) was calculated using the following equation:

$$E_a = E_{total} - E_s - E_m$$

where E_m, E_s and E_{total} are the bond energies of free molecules or ions, surface, and whole system, respectively.

2.6 Method of molecule dynamic (MD) simulation

The diffusion processes of molecules between two layers of graphene and on surface of graphene were simulated with MD method. A force field named PCFF30 was used in a Forcite package. This PCFF30 force field was built basing on empirical parameters and ab initio principle. The geometric optimizations were converged by following criteria: the maximum displacement should be than 1.0×10^{-5} Å and the energy tolerance should be less than 2.0×10^{-5} kcal mol^{-1} using a smart algorithm.

3. Results and discussion

Following our previously developed methods,[46] the sheets of holey-graphene were synthesized by directly heating the starting graphene in air under certain conditions. This scalable one-step synthesis process is illustrated in Figure 1a. The starting graphene that was used for the preparation of holey-graphene was bought from the company of Vorbeck Materials (the average size is 5-20 μm with 5-15 layers, information of the materials report from the company). The morphology of the starting graphene are shown Figure 1b and the BET measured surface area is 471 m^2 g^{-1} (shown in

our previous work).[46] Figures 1c and d show the TEM image and the high resolution TEM (HR-TEM) image of the starting graphene, respectively. After being heated at 430 ℃ for 3 hours (details in Methods Section), the graphene was transformed to holey-graphene. The detailed characterization in our previous work suggests that the noncrystalline areas on the pristine sheet of graphene were oxidized preferentially and converted to holes that distributed on the graphene surface after gasified to CO and CO_2.[40] The TEM image (Figure 1e) shows that the total morphology of holey-graphene has no obvious change compared with the starting graphene. The HR-TEM image (Figure 1f) shows that the holey-graphene possesses a large amount of holes. The statistical analysis indicates that the average size of the holes was 8.2 nm (inset of Figure 1e) with a density of 1.78×10^3 μm^{-2}. Our previous study shows that the more aggressive conditions in the thermal treatment, such as a longer residence time or a higher temperature will further gasify the remaining graphitic carbon and enlarge the holes.[46]

In this paper, we study the electrochemical properties of the as-synthesized holey-graphene as supporting materials for the Pt NPs catalysts. As composition, the properties of graphene and carbon black (commercial commonly-used supporting material) are also measured. Figure 2 shows the Raman spectra of carbon black, starting graphene and as-synthesized holey-graphene after being subtracted with baseline. The 5 curves for each sample is the 5 times measurement at different locations. When the graphene transform to holey-graphene, the average ratios of ID/IG (D band centered at 1333 cm^{-1} to G band centered at 1593 cm^{-1}) in the Raman spectra (Figures 2b and c) decreased from 1.8 to 1.3, indicating the improved graphitic crystallinity of holey-graphene relative to the starting graphene. In the starting graphene, the carbon atoms connect with with sp^3 bond (contributing to the D band) in the noncrystalline areas and defective regions. During the thermal

treatment, the carbons connected with sp^3 bonds are susceptible to oxidative removal via gasification, while, the carbons connected with sp^2 bonds (contributing to the G peak) remained stable. The improved graphitic crystallinity of holey-graphene also was confirmed by X-ray photoelectron spectra (XPS) analysis in our previous work.[46]

To study the feasibility of holey-graphene as supporting materials for metal NP catalysts, Pt NPs were synthesized and loaded on the holey-graphene due to their wide spread use and broad applicability. The details of synthesizing and loading of Pt NPs can be seen in the method section. Figure 3a shows the TEM image of Pt/H-G (Pt NPs loading on holey-graphene) and indicates that the size of the Pt NPs is uniform and around 3 nm. On the whole surface of the holey-graphene, the Pt NPs are evenly distributed. Figures 3b and c are two HR-TEM images, showing two typical area of Pt/H-G, where the arrows indicate the holes. The Pt NPs are seemingly preferential to locate at the step of graphene layers and the edge of the holes. The carbons at the step and edge are not fully connected with neighboring carbons and possess affinity to the Pt NPs. During the loading process of Pt NPs, the step and edge may limit the movement of Pt NPs on the surface of holey-graphene and attach together. The schematic image in Figure 3d illustrates Pt NPs loading on the holey-graphene. As comparison, carbon black and graphene are also used as supporting materials for Pt NPs. The loading methods and procedures for carbon black and graphene are same with holey-graphene (details are shown in Methods Section). Figures 4a and b are the TEM images of Pt NPs loaded on carbon black and graphene, respectively. The Pt NPs were distributed uniformly on the surface of carbon black and graphene. The loading ratios of Pt NPs on carbon black (Pt/C) and graphene (Pt/G) are the same as on holey-graphene (20%).

The electrochemical catalytic properties of Pt NPs loading on holey-graphene were evaluated.

First, in argon-purged 0.1 M $HClO_4$ aqueous solution, the cyclic voltammetry (CV) curves were recorded at room temperature. The CV curves obtained at the sweep rate of 50 mV/s for Pt/C, Pt/G, and Pt/HG are shown in Figure 5a. In the CV curves, two distinct potential regions are associated with the H_{upd} ($H^+ + e^- = H_{upd}$) desorption/adsorption between -0.2 and 0.1 V (vs Ag/AgCl) and the formation of OH adsorption layer ($2H_2O = OH_{ad} + H_3O^+ + e^-$) in the range of 0.4-1.0 V (vs Ag/AgCl), respectively. The electrochemical surface areas (ECSAs) of the 3 samples were calculated by measuring the charge collected in the H_{upd} desorption/adsorption region after double-layer correction and assuming a value of 210 C/cm^2 for the adsorption of a hydrogen monolayer on Pt surface.[51] The specific ECSAs (the ECSA per unit weight of Pt metal) of Pt/C, Pt/G, and Pt/HG are compared with histograms in Figure 5b. No matter the sweep rate, 50 mV/s or 20 mV/s, Pt NPs possess the largest specific ECSA when they are loaded on holey-graphene (Pt/HG). When the sweep rate decreased from 50 mV/s to 20 mV/s, the ECSAs increased 23%, 52%, and 15% for Pt/C, Pt/G, and Pt/HG, respectively. With a slow sweep rate the H^+ ions have more time to diffuse and attach with deeply embedded Pt NPs. Compared with Pt/C and Pt/G, Pt/HG shows both of the highest ECSA and the slowest increasing rate of ECSA. These results indicate that Pt nanoparticles are deeply embedded in graphene and are inhibited to accessing H^+ ions. The carbon black is better than graphene and the holey graphene exhibits the best properties.

The methanol oxidation reaction (MOR) was selected as the targeted reaction system to investigate the electrocatalytic properties of holey-graphene as a supporting material. By using similar methods as our previous work,[8,52] the CV curves of MOR catalyzed by Pt/C, Pt/G, and Pt/HG, in 0.5 M CH_3OH + 0.1 M $HClO_4$ aqueous solution at a scan rate of 10 mV/s were obtained and are shown in Figure 5c. The similar CV curves for the three catalysts suggest the same reaction pathway.

The Pt NPs show improved catalytic activity, when the holey-graphene is used as a supporting material. Considering the normalized peak current against the mass, the Pt/HG has a mass activity of 65 $\mu A/\mu g_{Pt}$ which is 2.5 times greater than Pt/C and 6.1 times greater than Pt/G. The onset potentials for Pt/C, Pt/G, and Pt/HG are 0.32 V, 0.31 V, and 0.29 V, and the oxidation peaks for them are 0.63 V, 0.64 V, and 0.66 V, respectively. The ratio of forward and reverse peak current densities can demonstrate the tolerance of catalyst to the accumulation of carbonaceous species. The ratios calculated from the CV curves for Pt/C, Pt/G, and Pt/HG are 2.8, 2.1, and 1.6, respectively. The Pt/HG still possesses the highest catalytic activity for MOR when the concentration of methanol and scan rate increase to 1 M and 20 mV/s. The mass activities of Pt/C, Pt/G and Pt/HG for the MOR in the two conditions are summarized and compared with the histograms in Figure 5d. These results indicate that holey-graphene can greatly improve the catalytic properties of Pt NPs as supporting materials.

The properties of holey-graphene as supporting materials were further investigated in more conditions. Figure 6a shows the CV curves of MOR catalyzed by Pt/HG with different concentrations of methanol at constant scan rate of 20 mV/s. The peak current increases with the increasing of methanol concentration, indicating that more methanol molecules are oxidized in per circle. As comparison, the CV curves measured with same conditions for Pt/C and Pt/G. The peak currents of the three catalysts with different methanol concentrations are summarized and compared in Figure 6b. At any methanol concentration, Pt/HG shows the highest catalytic activity. At the same time, Pt/HG possesses the highest slope of peak current versus methanol concentration. Similarly, when the scan rate was kept at 10 mV/s and the methanol concentration increases from 0.1 M to 3.0 M, same result is obtained as that at 20 mV/s.

When the concentration of methanol was kept at 0.5 M and the scan rate increased from 5 mV/s to 100 mV/s, the obtained CV curves for Pt/HG are shown in Figure 6c. With the increase of scan rate, the electrocatalytic current become high. Compared with Pt/C and Pt/G, Pt/HG possesses the largest increasing rate of peak current versus the square root of the scan rate (Figure 6d). The slopes of the fitting lines for peak current versus the square root of the scan rate are 3.6, 3.2 and 2.6 $\mu A/(mV/s)^{1/2}$ for Pt/HG, Pt/C, and Pt/G, respectively. By keeping the methanol concentration at 1.0 M and changing the scan rate from 5 mV/s to 100 mV/s, Pt/HG samely shows the largest rate increase of peak current versus the square root of the scan rate.

The surficial poisoning process of the three catalysts was evaluated using chronoamperometry in the solution of 0.5 M CH_3OH + 0.1 M $HClO_4$at a constant potential of 0.65 V (vs Ag/AgCl) for 1000 s. As shown in Figure 7, the polarization currents for all of the 3 catalysts decrease rapidly due to the formation of intermediate species during the MOR process. Compared with Pt/C and Pt/G, Pt/HG shows the higher reaction current during the poisoning process, indicating that Pt/HG possesses higher stability property in the MOR. The durability of the catalysts was further investigated in an accelerated durability test (ADT), same as that performed in our previous work, by applying linear potential sweeps from 0.4 to 0.9 V (vs Ag/AgCl) at 50 mV/s in oxygen-saturated 0.1 M 0.1 M $HClO_4$ solution. Figures 8a-c show the CV curves of Pt/C, Pt/G, and Pt/HG catalysts before and after 1000 ADT cycles. During the process, the losses of ECSA are 19 %, 13%, and 11% for the Pt/C, Pt/G, and Pt/HG catalysts, respectively. These results further indicate that Pt/HG have enhanced durability in the electrochemistry catalysis system.

The diffusion of ions on the electrode was analyzed using the Nyquist electrochemical impedance spectroscopy (EIS) plots. The EIS plots of Pt/C, Pt/G, and Pt/HG decorated electrodes are

shown in Figure 9. At the high frequency range (Figure 9b), the resistance capacitor semicircle was no longer clearly obtained after the graphene or holey-graphene being loaded with Pt NPs, although it appeared in the pure graphene or holey-graphene as shown in our previous work. This may indicate that the conductivity become increase after Pt NPs loading. The curves in the low frequency range of the EIS plots (Figure 9a) show that the impediment of ions on Pt/HG decorated electrodes is lower than that of Pt/C and Pt/G.

To explain the experimental results, the method of density functional theory (DFT) was used to calculate the adsorption energy of reactants, such as CH_3OH, OH^- and $HCOO^-$, on the surface of the catalysts. During the MOR process, there are many transition states that occur on the metal catalyst surface.[53] The premise for the reaction catalyzed on the metal surface is that the reactants and their products should be adsorbed on the surface of the catalysts. Using similar DFT methods as that in our previous work,[54,55] the adsorption energy of CH_3OH, OH^- and $HCOO^-$ on a Pt crystal surface and graphene were calculated. The Pt NPs usually are covered by the low index crystalline surface, i.e. (100) and (111) facets. In the MOR system, the Pt (100) possesses the higher catalytic property than Pt (111) surface.[52] Thus, in the DFT calculation, Pt (100) was selected and studied. Figure 10 shows the top and side views of the most likely configurations of the $HCOO^-$ ion on Pt(100) surface, one layer of graphene, Pt(100) surface covered by one layer of graphene (1LG/Pt), and Pt(100) surface covered by two layer of graphene (2LG/Pt) (fully optimized based on DFT). The adsorption energies are tabulated and shown in Table 1. The Pt(100) surface possesses the highest adsorption energies for all of the molecules and ions compared with the graphene and the graphene covered Pt(100) surface (1LG/Pt and 2LG/Pt). Although the adsorption energies of molecules or ions are obviously higher on 1LG/Pt than that on pure graphene and 2LG/Pt, they are still much lower than

pure Pt crystal. This result indicates that the covering of platinum by graphene will prevent the reactants and their products in the MOR process to be adsorbed on the surface of the catalyst.

The molecular dynamic (MD) simulation was further to investigate the diffusion of molecules on or between the layers of graphene. Figures 11a and b are the MD simulation results of the diffusion of one methanol molecule between two layers of 3 nm × 3 nm graphene and diffusion on their surface. Figure 11c shows that much higher energy is needed for the diffusion of methanol molecule between layers of graphene than that diffusion on their surface.

Combined with the results of the theoretical calculation, the experimental results can be explained. As schematically illustrated by Figure 12a, when the graphene is used as supporting material for Pt NPs, they will wrap the Pt NPs and prevent reactant adsorption (Figure 10). On the other hand, the restacking of graphene due to the strong interaction formed by the 'π' electrons between layers of graphene will limit molecule and ion diffusion between layers of graphene (Figure 11). Because Pt NPs are deeply wrapped by graphene, some Pt NPs cannot access the reactants and some Pt NPs need a long time to access the reactants by diffusion of reactants through the layers of graphene. Thus, in the electrocatalytic reaction, with higher scan rates, the ECSA and electrocatalytic activity of Pt NPs become worse using graphene as supporting material compared to holey-graphene used as supporting material. As illustrated by Figure 12b, using holey-graphene as supporting material allows reactants to diffuse through the holes to access the Pt NPs during the electrocatalytic reaction. Likewise, the products such as CO_2 in the MOR also will diffuse and release from the electrode by diffusing out of the holes of holey-graphene. At high concentrations of methanol, the methanol molecules can quickly diffuse through the holes of holey-graphene to the surface of Pt NPs and be electrocatalytically oxidized. Thus, with the increase methanol concentration, Pt/HG shows a

more quick increase in the electrocatalytic current than that of Pt/G and Pt/C.

4. Conclusions

In summary, this paper elucidates the effect of graphene and holey-graphene as supporting materials for Pt NPs catalysts on the methanol oxidation reaction. Although graphene as a catalyst support possesses high electrical conductivity, high specific surface area, and relatively good stability, the restacking of graphene layers wrap the Pt NP catalysts and limit accessing of reactants to the catalyst surface. To overcome the restacking problem of graphene, holey-graphene was developed and loaded with Pt NPs. By using a simple thermal treatment method, the holey-graphene could be scalable and low cost to synthesize. In the electrocatalytic reaction system, the reactants could easily diffuse through the holes on the holey-graphene and could access the Pt NP catalysts. Thus, the ECSA and electrocatalytic activity of the catalyst were greatly improved when using the holey-graphene as the supporting material when compared with carbon black or graphene. Our study provides a new route for enhancing the catalytic properties of noble metal NPs by using holey-graphene as the supporting material.

Acknowledgment

H. J. You acknowledges the programs supported by the Natural Science Foundation of Shaanxi Province (No. 2017JM5072), and the Fundamental Research Funds for the Central Universities (No. xjj2017102). J. X. Fang acknowledges the programs supported by the National Natural Science Foundation of China (No. 21675122). X.H. Han acknowledges the programs supported by Key Research Program of Shaanxi Province (2017ZDXM-GY-035) and Young Talent Support Plan of Xi'an Jiaotong University. X.H. Han also thanks the Fundamental Research Funds for the Central

Universities (1191329736, xjj2017076) and the State Key Laboratory of Electrical Insulation and Power Equipment (EIPE17306) for financial support.

References

[1] Gilroy K D, Ruditskiy A, Peng H C, Qin D and Xia Y N 2016 Bimetallic Nanocrystals: Syntheses, Properties, and Applications *Chem. Rev.* **116** 10414-10472

[2] Strasser P 2015 Catalysts by Platonic design *Science* **349** 379-380

[3] You H J, Yang S C, Ding B J and Yang H 2013 Synthesis of colloidal metal and metal alloy nanoparticles for electrochemical energy applications *Chem. Soc. Rev.* **42** 2880-2904

[4] Pedireddy S, Lee H K, Tjiu W W, Phang I Y, Tan H R, Chua S Q, Troadec C and Ling X Y 2014 One-step synthesis of zero-dimensional hollow nanoporous gold nanoparticles with enhanced methanol electrooxidation performance *Nat. Commun.* **5** 5947

[5] You H J and Fang J X 2016 Particle-mediated nucleation and growth of solution-synthesized metal nanocrystals: A new story beyond the LaMer curve *Nano Today* **11** 145-167

[6] Chen C *et al* 2014 Highly Crystalline Multimetallic Nanoframes with Three-Dimensional Electrocatalytic Surfaces *Science* **343** 1339-1343

[7] Huang X Q *et al* 2015 High-performance transition metal-doped Pt3Ni octahedra for oxygen reduction reaction *Science* **348** 1230-1234

[8] You H J, Zhang F L, Liu Z and Fang J X 2014 Free-Standing Pt-Au Hollow Nanourchins with Enhanced Activity and Stability for Catalytic Methanol Oxidation *ACS Catal.* **4** 2829-2835

[9] Li T, You H J, Xu M W, Song X P and Fang J X 2012 Electrocatalytic Properties of Hollow Coral-like Platinum Mesocrystals *ACS Appl. Mater. Interfaces* **4** 6941-6947

[10] Zhuang L N, Wang W J, Hong F, Yang S C, You H J, Fang J X and Ding B J 2012 Porous

platinum mesoflowers with enhanced activity for methanol oxidation reaction *J. Solid State Chem.* **191** 239-245

[11] Fu G T, Xia B Y, Ma R G, Chen Y, Tang Y W, Lee J M 2015 Trimetallic PtAgCu@PtCu core@shell concave nanooctahedrons with enhanced activity for formic acid oxidation reaction *Nano Energy* **12** 824-832

[12] Peng Z M, You H J and Yang H 2010 An Electrochemical Approach to PtAg Alloy Nanostructures Rich in Pt at the Surface *Adv. Funct. Mater.* **20** 3734-3741

[13] Wang H F and Liu Z P 2008 Comprehensive mechanism and structure-sensitivity of ethanol oxidation on platinum: New transition-state searching method for resolving the complex reaction network *J. Am. Chem. Soc.* **130** 10996-11004

[14] Du C, Gao X H, Zhuang Z H, Cheng C F, Zheng F Q, Li X K and Chen W 2017 Epitaxial growth of zigzag PtAu alloy surface on Au nano-pentagrams with enhanced Pt utilization and electrocatalytic performance toward ethanol oxidation reaction *Electrochim. Acta* **238** 263-268.

[15] Jha N, Reddy A L M, Shaijumon M M, Rajalakshmi N and Ramaprabhu S 2008 Pt-Ru/multi-walled carbon nanotubes as electrocatalysts for direct methanol fuel cell *Int. J. Hydrog. Energy* **33** 427-433

[16] Do I and Drzal L T 2014 Ionic Liquid-Assisted Synthesis of Pt Nanoparticles onto Exfoliated Graphite Nanoplatelets for Fuel Cells *ACS Appl. Mater. Interfaces* **6** 12126-12136

[17] Sharma S and Pollet B G 2012 Support materials for PEMFC and DMFC electrocatalysts-A review *J. Power Sources* **208** 96-119

[18] Antolini E and Gonzalez E R 2009 Polymer supports for low-temperature fuel cell catalysts *Appl. Catal. A-Gen.* **365** 1-19

[19] Roy S C, Christensen P A, Hamnett A, Thomas K M and Trapp V 1996 Direct methanol fuel cell cathodes with sulfur and nitrogen-based carbon functionality *J. Electrochem. Soc.* **143** 3073-3079

[20] Shao Y Y, Yin G P and Gao Y Z 2007 Understanding and approaches for the durability issues of Pt-based catalysts for PEM fuel cell *J. Power Sources* **171** 558-566

[21] Solla-Gullon J, Lafuente E, Aldaz A, Martinez M T and Feliu J M 2007 Electrochemical characterization and reactivity of Pt nanoparticles supported on single-walled carbon nanotubes *Electrochim. Acta* **52** 5582-5590

[22] Hsin Y L, Hwang K C and Yeh C T 2007 Poly(vinylpyrrolidone)-modified graphite carbon nanofibers as promising supports for PtRu catalysts in direct methanol fuel cells. *J. Am. Chem. Soc.* **129** 9999-10010

[23] Maiyalagan T 2009 Pt-Ru nanoparticles supported PAMAM dendrimer functionalized carbon nanofiber composite catalysts and their application to methanol oxidation. *J. Solid State Electrochem.* **13** 1561-1566

[24] Song S Q, Liang Y R, Li Z H, Wang Y, Fu R W, Wu D C and Tsiakaras P 2010 Effect of pore morphology of mesoporous carbons on the electrocatalytic activity of Pt nanoparticles for fuel cell reactions *Appl. Catal. B-Environ.* **98** 132-137

[25] Wang L, Tian C G, Mu G, Zhang H X and Fu H G 2012 Facile synthesis of Pt nanocrystals/graphene composite with excellent methanol electro-oxidation performance *Mater. Res. Bull.* **47** 4311-4315

[26] Li Y J, Zhu E B, McLouth T, Chiu C Y, Huang X Q and Huang Y 2012 Stabilization of High-Performance Oxygen Reduction Reaction Pt Electrocatalyst Supported on Reduced Graphene

Oxide/Carbon Black Composite *J. Am. Chem. Soc.* **134** 12326-12329

[27] Li S S, Lv J J, Teng L N, Wang A J, Chen J R and Feng J J 2014 Facile Synthesis of PdPt@Pt Nanorings Supported on Reduced Graphene Oxide with Enhanced Electrocatalytic Properties *ACS Appl. Mater. Interfaces* **6** 10549-10555

[28] Mondal A and Jana N R 2015 Effect of size and oxidation state of platinum nanoparticles on the electrocatalytic performance of graphene-nanoparticle composites *RSC Adv.* **5** 85196-85201

[29] Vinayan B P, Nagar R and Ramaprabhu S 2012 Synthesis and investigation of mechanism of platinum-graphene electrocatalysts by novel co-reduction techniques for proton exchange membrane fuel cell applications *J. Mater. Chem.* **22** 25325-25334

[30] Guo S J, Dong S J and Wang E K Three-Dimensional Pt-on-Pd Bimetallic Nanodendrites Supported on Graphene Nanosheet: Facile Synthesis and Used as an Advanced Nanoelectrocatalyst for Methanol Oxidation *ACS Nano* **4** 547-555

[31] Bai S, Wang C M, Deng M S, Gong M, Bai Y, Jiang J and Xiong Y J 2014 Surface Polarization Matters: Enhancing the Hydrogen-Evolution Reaction by Shrinking Pt Shells in Pt-Pd-Graphene Stack Structures *Angew. Chem.-Int. Edit.* 53 12120-12124

[32] Lu Y Z, Jiang Y Y and Chen W 2014 Graphene nanosheet-tailored PtPd concave nanocubes with enhanced electrocatalytic activity and durability for methanol oxidation *Nanoscale* **6** 3309-3315

[33] Sun L T, Wang H J, Eid K, Alshehri S M, Malgras V, Yamauchi Y and Wang L 2016 One-Step Synthesis of Dendritic Bimetallic PtPd Nanoparticles on Reduced Graphene Oxide and Its Electrocatalytic Properties *Electrochim. Acta* **188** 845-851

[34] Kim Y, Noh Y, Lim E J, Lee S, Choi S M and Kim W B 2014 Star-shaped Pd@Pt core-shell catalysts supported on reduced graphene oxide with superior electrocatalytic performance *J. Mater.*

Chem. A **2** 6976-6986

[35] Du S F and Lu Y X 2014 Steinberger-Wilckens, R. PtPd nanowire arrays supported on reduced graphene oxide as advanced electrocatalysts for methanol oxidation *Carbon* **79** 346-353

[36] Yuk J M, Park J, Ercius P, Kim K, Hellebusch D J, Crommie M F, Lee J Y, Zettl A and Alivisatos A P 2012 High-Resolution EM of Colloidal Nanocrystal Growth Using Graphene Liquid Cells *Science* **336** 61-64

[37] Wang X Z, Xiao Y H, Su D C, Xu S G, Zhou L M, Wu S D, Han L F, Fang S M and Cao S K 2016 Hierarchical porous cobalt monoxide nanosheet@ultrathin manganese dioxide nanosheet core-shell arrays for high-performance asymmetric supercapacitor *Int. J. Hydrog. Energy* **41** 13540-13548

[38] Xiao Y H, Su D C, Wang X Z, Wu S D, Zhou L M, Sun Z H, Wang Z X, Fang S M and Li F 2017 Ultrahigh energy density and stable supercapacitor with 2D NiCoAl Layered double hydroxide *Electrochim. Acta.* **253** 324-332

[39] Xiao Y H, Su D C, Wang X Z, Wu S D, Zhou L M, Fang S M and Li F 2018 Layered double hydroxides with larger interlayer distance for enhanced pseudocapacitance *Sci. China-Mater.* **61** 263-272

[40] Niu Z Q, Chen J, Hng H H, Ma J and Chen X D 2012 A Leavening Strategy to Prepare Reduced Graphene Oxide Foams *Adv. Mater.* **24** 4144-4150

[41] Choi B G, Yang M, Hong W H, Choi J W and Huh Y S 2012 3D Macroporous Graphene Frameworks for Supercapacitors with High Energy and Power Densities *ACS Nano* **6** 4020-4028

[42] Palaniselvam T, Kashyap V, Bhange S N, Baek J B and Kurungot S 2016 Nanoporous Graphene Enriched with Fe/Co-N Active Sites as a Promising Oxygen Reduction Electrocatalyst for

Anion Exchange Membrane Fuel Cells *Adv. Funct. Mater.* **26** 2150-2162

[43] Zhou L H, Wang Y X, Tang J, Li J X, Wang S L and Wang Y 2017 Facile synthesis of holey graphene-supported Pt catalysts for direct methanol electro-oxidation. *Microporous Mesoporous Mat.* **247** 116-123

[44] Walsh E D, Han X G, Lacey S D, Kim J W, Connell J W, Hu L B and Lin Y 2016 Dry-Processed, Binder-Free Holey Graphene Electrodes for Supercapacitors with Ultrahigh Areal Loadings *ACS Appl. Mater. Interfaces* **8** 29478-29485

[45] Lin Y, Moitoso B, Martinez-Martinez C, Walsh E D, Lacey S D, Kim J W, Dai L M, Hu L B and Connell J W 2017 Ultrahigh-Capacity Lithium-Oxygen Batteries Enabled by Dry-Pressed Holey Graphene Air Cathodes *Nano Lett.* **17** 3252-3260

[46] Han X G *et al* 2014 Scalable Holey Graphene Synthesis and Dense Electrode Fabrication toward High-Performance Ultracapacitors *ACS Nano* **8** 8255-8265

[47] You H J, Peng Z M, Wu J B and Yang H 2011 Lattice contracted AgPt nanoparticles *Chem. Commun.* **47** 12595-12597

[48] You H J, Wang W J and Yang S C 2014 A Universal Rule for Organic Ligand Exchange *ACS Appl. Mater. Interfaces* **6** 19035-19040

[49] Delley B 2000 From Molecules to Solids with the DMol(3) Approach *J. Chem. Phys.* **113** 7756-7764

[50] Perdew J P and Wang Y 1992 Accurate and Simple Analytic Representation of the Electron-Gas Correlation-Energy *Phys. Rev. B* **45** 13244-13249

[51] Schmidt T J, Gasteiger H A, Stab G D, Urban P M, Kolb D M and Behm R J 1998 Characterization of High-Surface Area Electrocatalysts Using a Rotating Disk Electrode

Configuration *J. Electrochem. Soc.* **145** 2354-2358

[52] Peng Z M, You H J, Wu J B and Yang H 2010 Electrochemical Synthesis and Catalytic Property of Sub-10 nm Platinum Cubic Nanoboxes *Nano Lett.* **10** 1492-1496

[53] Zope B N, Hibbitts D D, Neurock M and Davis R J 2010 Reactivity of the Gold/Water Interface During Selective Oxidation Catalysis *Science* **330** 74-78

[54] Yang Z B, Zhang L, You H J, Li Z Y and Fang J X 2014 Particle-Arrayed Silver Mesocubes Synthesized via Reducing Silver Oxide Mesocrystals for Surface-Enhanced Raman Spectroscopy *Part. Part. Syst. Charact.* **31** 390-397

[55] You H J, Liu X T, Liu H Z and Fang J X Theoretical Description of the Role of Amine Surfactant on the Anisotropic Growth of Gold Nanocrystals *CrystEngComm* **18** 3934-3941

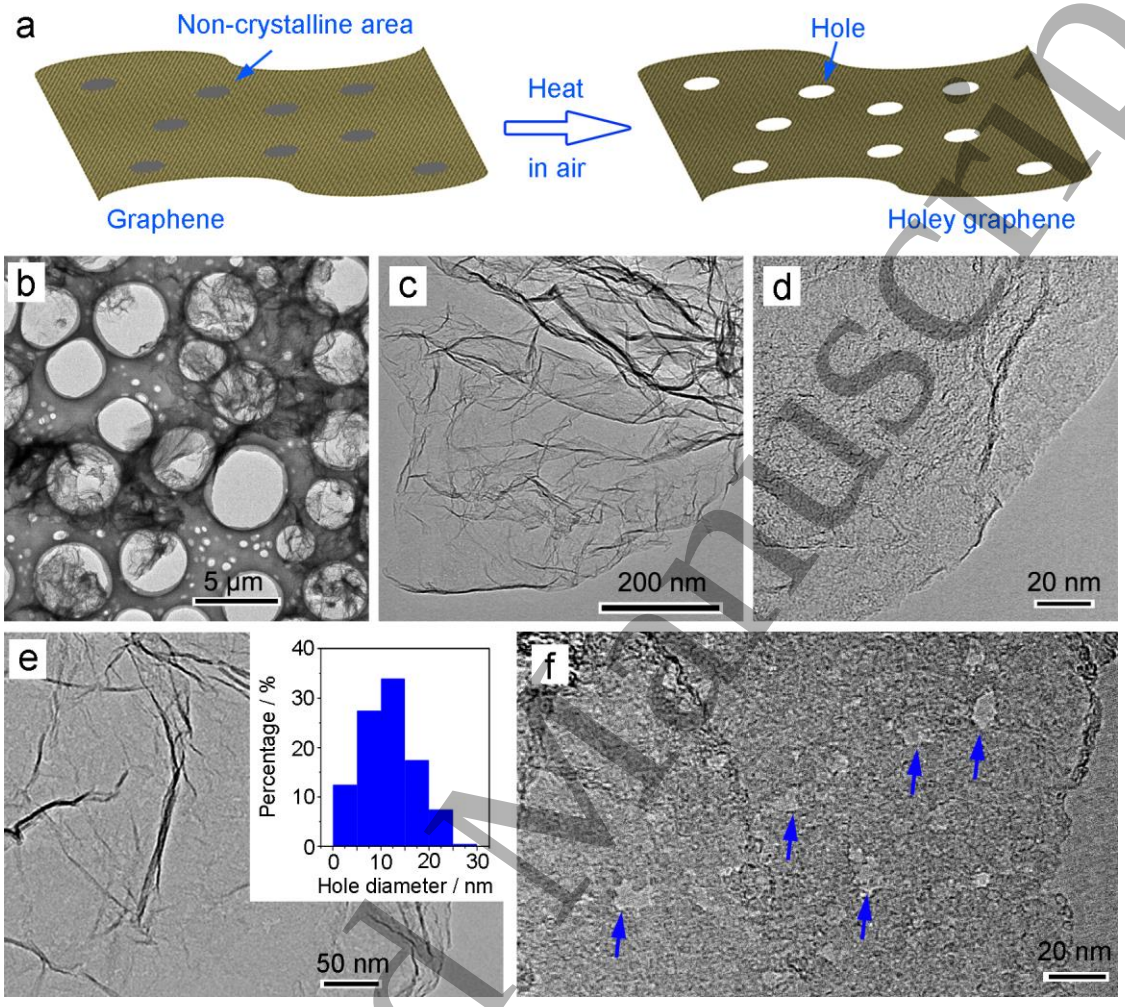

Figure 1. (a) Schematic of holey-graphene synthesis with thermal treatment. (b) TEM image of the starting graphene in a large area scope. The (c) low and (d) high magnified TEM images of starting graphene. The (e) low and (f) high magnified TEM images of holey graphene with the holes being indicated by arrows. The inset image in (e) is the hole diameter distribution statistics for the holey-graphene.

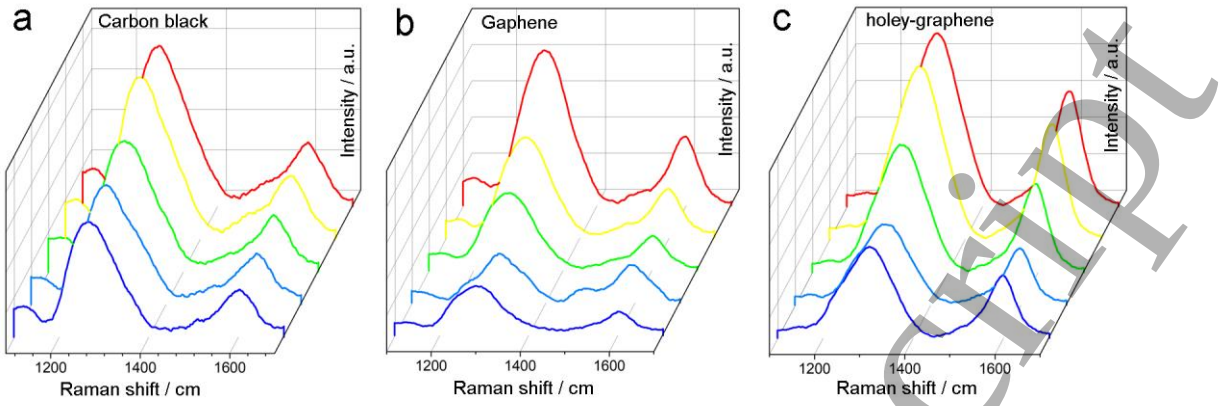

Figure 2. The Raman spectra images for (a) carbon black, (b) starting graphene, and (c) holey-graphene.

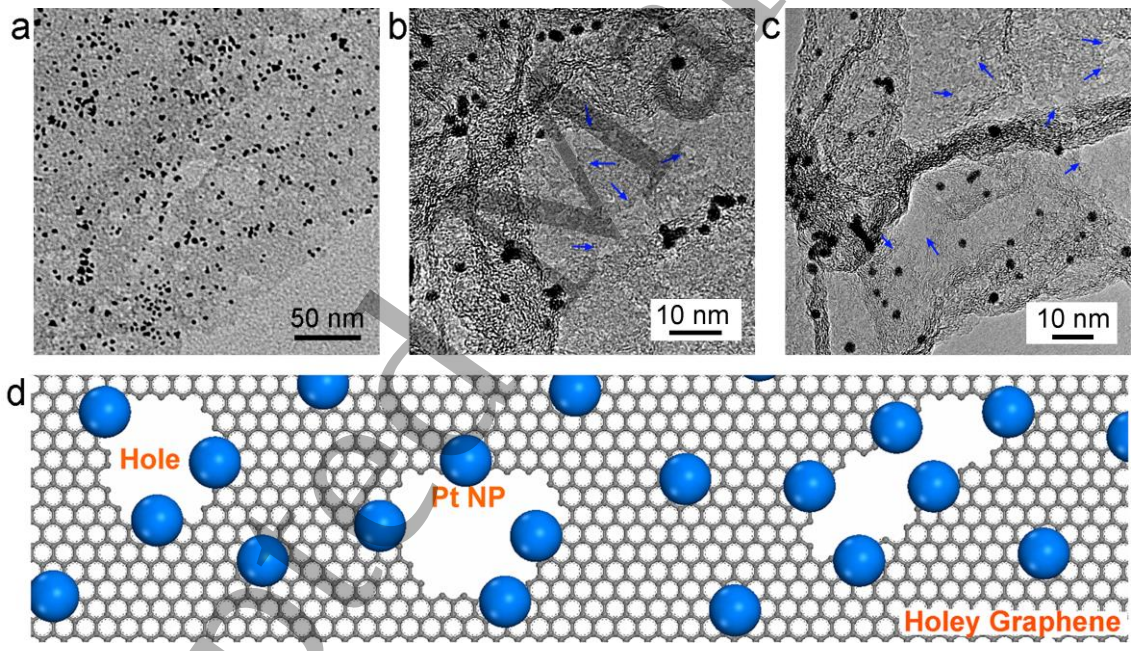

Figure 3. (a) The TEM images of Pt NPs loaded on the holey graphene. (b, c) Two typical HR-TEM images of Pt NPs loaded on the holey graphene. The arrows in (b, c) indicate the holes of holey graphene. (d) Schematic image of Pt nanoparticles (NPs) loaded on holey graphene.

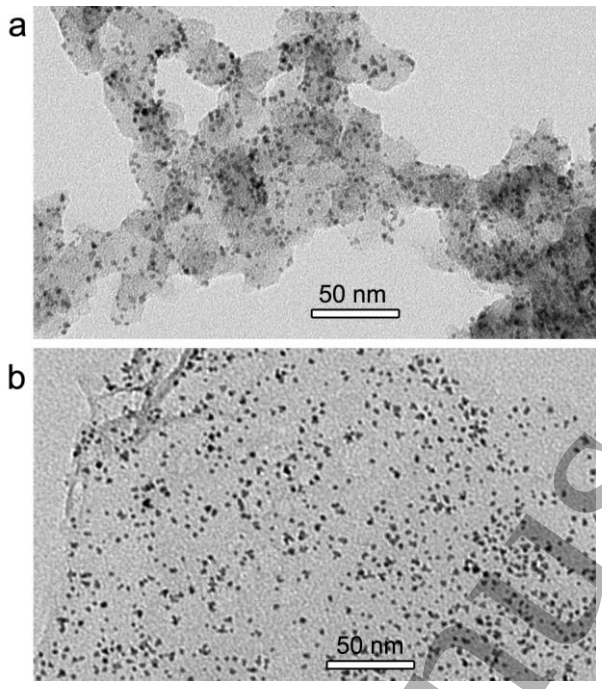

Figure 4. TEM images of (a) Pt nanoparticles loading on carbon black and (b) TEM images of Pt nanoparticles loading on graphene.

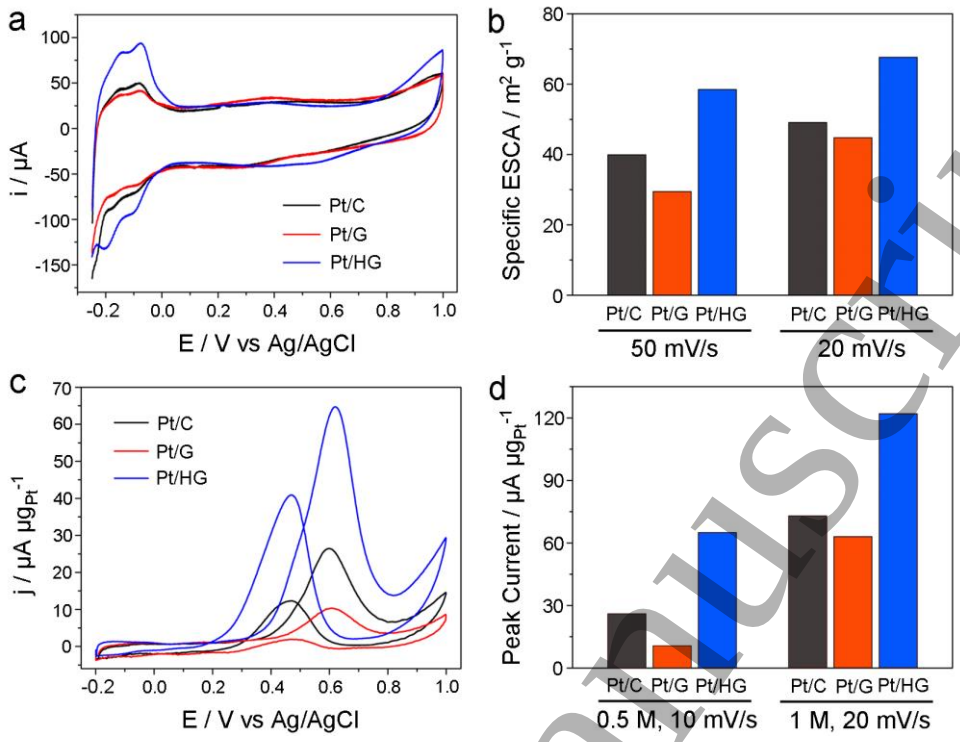

Figure 5. (a) The CV curves obtained for Pt nanoparticles (NPs) loaded on carbon (Pt/C), graphene (Pt/G), and holey graphene (Pt/HG) in 0.1 M $HClO_4$ solution at 50 mV/s, respectively. (b) Histograms of the specific electrochemical surface areas (ECSAs) for the three catalyst systems obtained with 50 mV/s and 20 mV/s sweep rates. (c) Methanol oxidation reaction (MOR) catalyzed by the three catalyst systems in 0.1 M $HClO_4$ + 0.5 M CH_3OH solution at 10 mV/s. (d) Histograms of the activities of the three catalyst systems for the MOR at the two conditions.

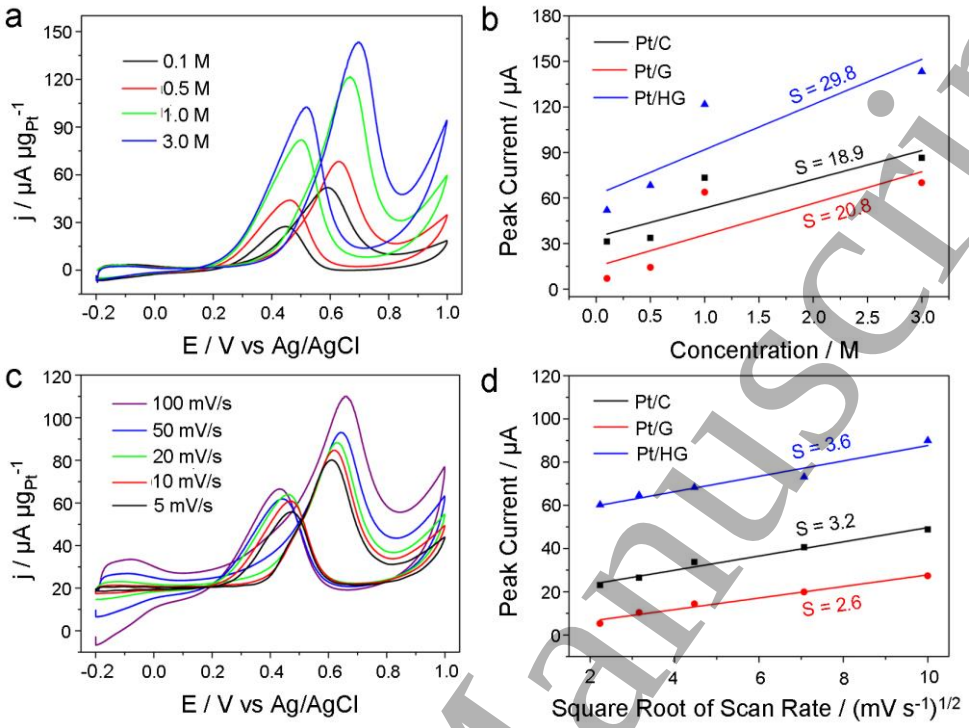

Figure 6. (a) Methanol oxidation reaction (MOR) catalyzed by the Pt/HG in solution with different concentrations of methanol at 20 mV/s. (b) The calibration plot of MOR peak current density versus concentration of methanol for three different catalyst systems. (c) MOR catalyzed by the Pt/HG with different scan rates in 0.1 M $HClO_4$ + 0.5 M CH_3OH solution. (d) Dependence of the peak current of the three catalyst systems on the square root of the potential scan rate for the MOR. The signal 'S' in (b) and (d) indicate the slop of the fitting lines.

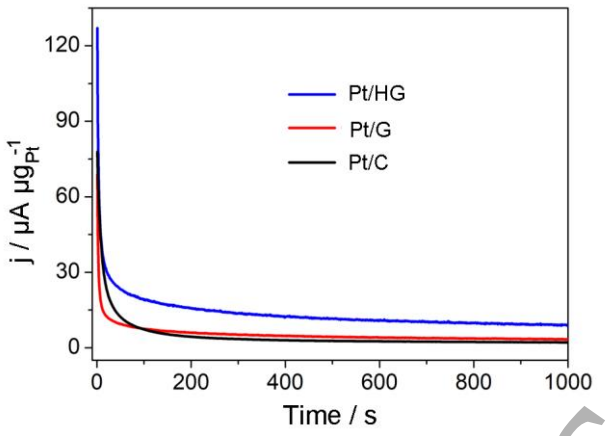

Figure 7. The chronoamperometric response of oxidation of methanol in 0.1 M $HClO_4$ + 0.5 M CH_3OH solution at a constant potential of 0.65 V (vs Ag/AgCl).

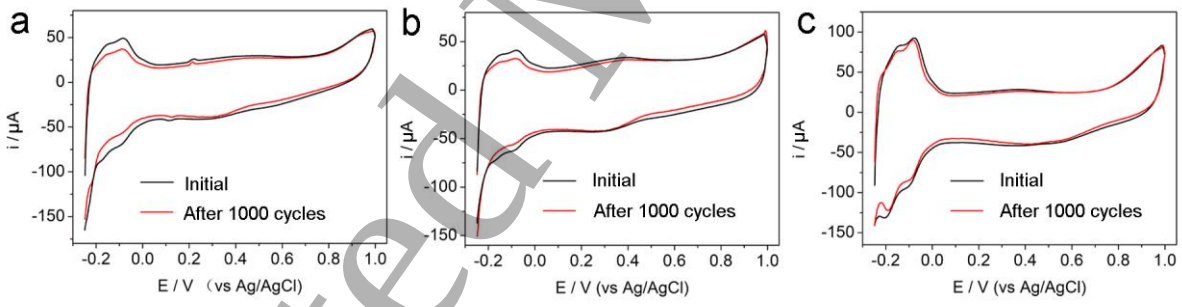

Figure 8. The CV curves of (a) Pt/C, (b) Pt/G and (c) Pt/HG obtained in 0.1 M $HClO_4$ solution at 50 mV/s before and after an accelerated durability test (ADT).

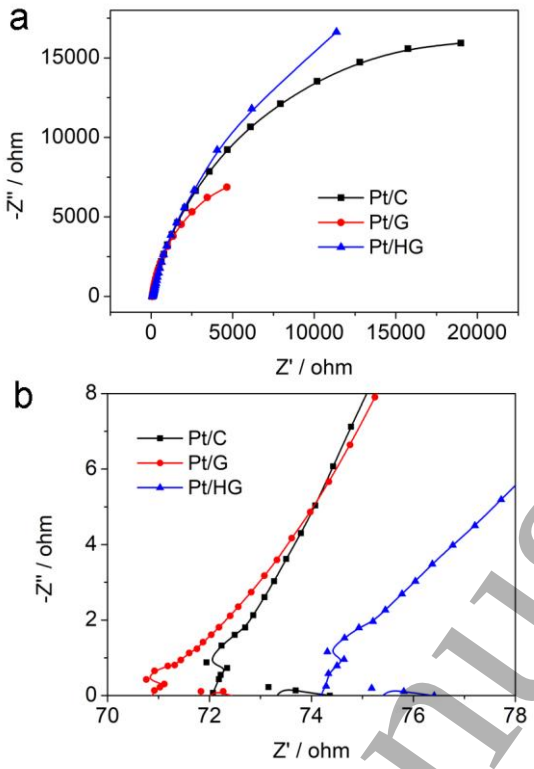

Figure 9. Nyquist EIS plots of Pt/C, Pt/G, and Pt/HG in (a) the full of range and (b) the high-frequency range.

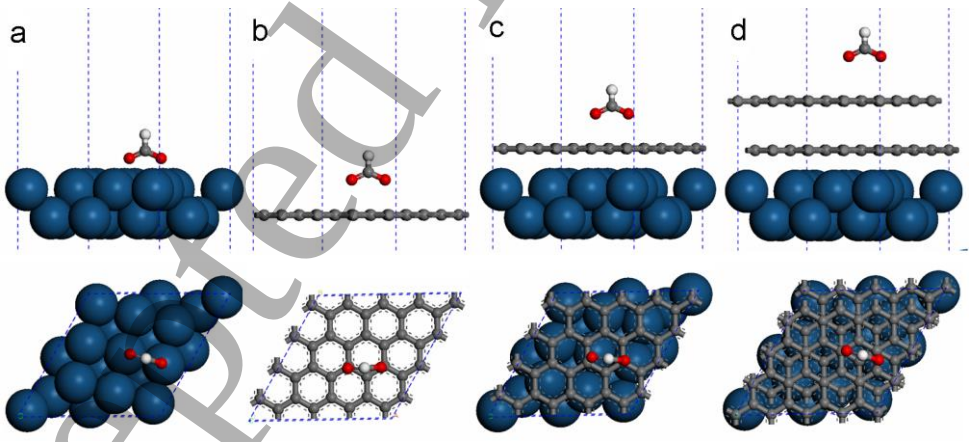

Figure 10. Optimized configurations of $HCOO^-$ ions adsorbed on (a) Pt(100), (b) graphene, (c) one layer of graphene covered Pt(100), and (d) two layers of graphene covered Pt(100) surfaces in a periodic cell using DFT method.

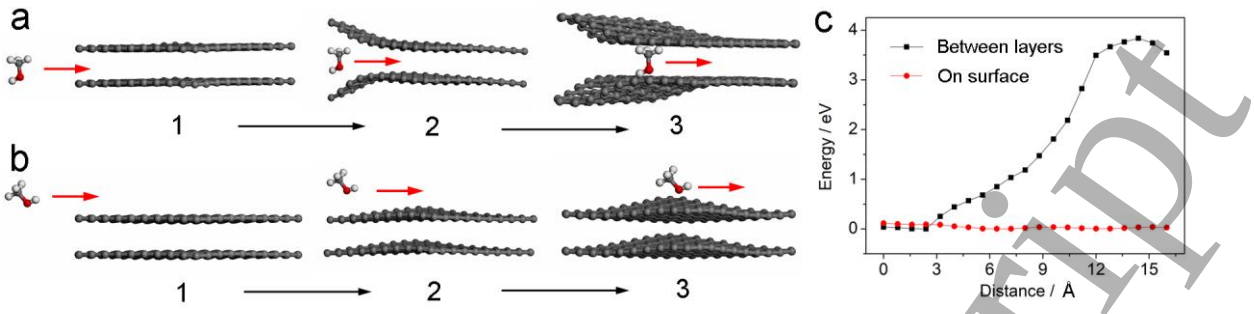

Figure 11. The molecular dynamic (MD) simulation of methanol molecule diffusion (a) between two layers of graphene and (b) on the surface of graphene. (c) The energy change during the MD process.

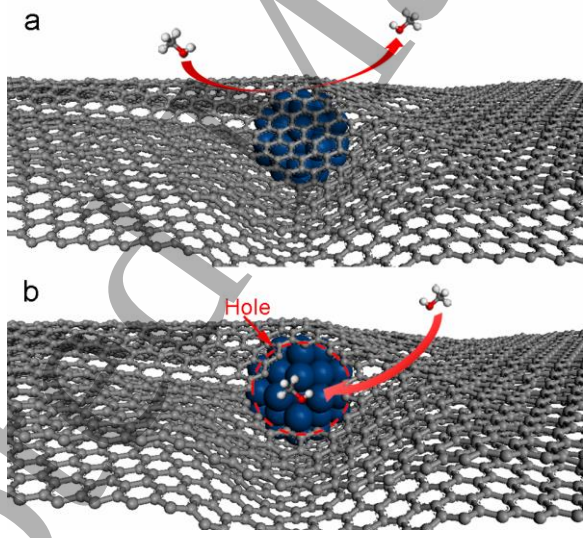

Figure 12. Schematic image illustrating the mechanism of holey-graphene (bottom, b) improving the electrocatalytic properties as a supporting material when compared with graphene (top, a).

Table 1. Adsorption Energy (E_a) of CH_3OH Molecule, OH^- Ion and $HCOO^-$ ion, Obtained from DFT Calculations, onto Pt(100), Graphene, Pt(100) Surface Covered by one layer of Graphene (1LG/Pt), and Pt(100) Surface Covered by Two Layers of Graphene. (Units: eV)

	CH_3OH molecule	OH^- ion	$HCOO^-$ ion
Pt(100)	-0.355	-1.636	-1.232
Graphene	-0.080	-0.046	-0.049
1LG/Pt	-0.116	-0.066	-0.095
2LG/Pt	-0.097	-0.047	-0.093